Bull. Mater. Sci. (2022) 45:100
https://doi.org/10.1007/s12034-022-02669-6

Facile electrochemical detection of morpholine in boiler water with carbon nanostructures: a comparative study of graphene and carbon nanotubes

SANAIR MASSAFRA DE OLIVEIRA[1,2], KELLY LEITE DOS SANTOS CASTRO ASSIS[1,2], VICTOR MAGNO PAIVA[1], MAZDAK HASHEMPOUR[4,5], MASSIMILIANO BESTETTI[3], JOYCE R DE ARAÚJO[2] and ELIANE D'ELIA[1,*]

[1]Institute of Chemistry, Federal University of Rio de Janeiro, University City, Rio de Janeiro 21941-909, Brazil
[2]National Institute of Metrology, Quality and Technology, Duque de Caxias 25250-020, Brazil
[3]Department of Chemistry, Materials and Chemical Engineering 'Giulio Natta', Politecnico di Milano, 20133 Milan, Italy
[4]Department of Materials Science and Engineering, Sharif University of Technology, 14588-89694 Tehran, Iran
[5]Institute of Water and Energy, Sharif University of Technology, 11365-8639 Tehran, Iran
*Author for correspondence (eliane@iq.ufrj.br)

MS received 22 July 2021; accepted 31 December 2021

Abstract. Two electrochemical sensors based on modified glassy carbon electrodes with carbon nanostructures as graphene (GCE-EG) and carbon nanotubes (GCE–CNT) were evaluated for morpholine analysis. The carbon nanostructures were obtained and characterized using X-ray photoelectron spectroscopy, Raman spectroscopy, X-ray diffraction, transmission electron microscopy, high-resolution transmission electron microscopy and cyclic voltammetry. All spectroscopic and microscopic techniques confirmed the procurement of graphene and CNT. The electrochemical studies proved the efficient behaviour of both electrodes GCE–EG and GCE–CNT in sensing and detection of morpholine via differential pulse voltammetry. The area of the anodic peaks was correlated with the concentration of the analyte. It was observed that the implementation of a thin film of EG and CNT on the GCE promoted the electrocatalytic activity towards morpholine electro-oxidation, and a considerable increase in the corresponding oxidation peak was observed in both cases. Theoretical detection limits of 1.0 and 1.3 mg l^{-1} were obtained for GCE–EG and GCE–CNT, respectively. These merit figures, both satisfactorily meet the requirements of the Food and Drug Administration for morpholine detection in real applications. Finally, the sample recovery for GCE–EG and GCE–CNT sensors were, respectively, 107 and 103%, at 20.0 mg l^{-1} morpholine in the boiler water.

Keywords. Morpholine; graphene; carbon nanotube; electro-oxidation.

1. Introduction

Morpholine (tetrahydro-2H-1,4-oxazine) is a secondary heterocyclic amine with an ether functional group [1]. Under normal temperature and pressure conditions, it is a colourless liquid, hygroscopic, totally miscible in water, and with a characteristic odour of amines [1,2]. This organic molecule presents great industrial importance in a wide range of applications, such as coating agent for fruits and vegetables, corrosion inhibitor in the oil and food industries, vulcanization accelerator in rubber production, catalyst, antioxidants and bactericide in pharmaceutics, optical bleach in the paper industry, cellulose solvent in the textile industry, pH controller in power plants and as a solvent in several other manufacturing processes [3,4].

Because it is a water-soluble molecule, significant amounts of it are released through industrial effluents into the environment, where they would undergo chemical or microbiological nitrosation processes, leading to the formation of N-nitrosomorpholine (NMOR), a highly carcinogenic compound [1,5]. NMOR could be present in a wide variety of products such as food, drinks, medication, cosmetics, biological samples such as saliva, blood and tissues, pesticides, rubber products, environmental samples such as air, soil and water effluents, among others [3,6].

The treatment of boiler water, composed of $CaCO_3$, Na_2SO_3, Na_3PO_4 and $FeCl_3$, with morpholine is efficient for

Supplementary Information: The online version contains supplementary material at https://doi.org/10.1007/s12034-022-02669-6.

Published online: 04 June 2022

corrosion protection purposes, due to its comparable volatility with water. That is, the concentration of morpholine is evenly distributed in both water and steam phases, and its pH adjustment function is distributed throughout the steam plant, thus promoting corrosion protection. Although morpholine is not considered toxic for humans in common exposure levels, some studies showed that morpholine was irritating to the digestive tract when orally administered to rats, which can induce stomach and small intestine haemorrhage in guinea pigs and rats. In this way, the Food and Drug Administration (FDA) determined that the concentration of such inhibitors should not exceed 10 mg l^{-1} and its use is not allowed in the European Union and the United Kingdom for being a precursor of NMOR [7–10]. Therefore, the development of a simple high-throughput analytical method to monitor morpholine is of great importance.

Determination of morpholine is reported in the literature in different matrices [10–15] and techniques, such as liquid chromatographic [16], gas chromatographic [17] and spectrophotometry [16]. Although chromatographic methods are sensitive, the costs of equipment maintenance are high, and derivatization is necessary. In contrast, electroanalytical techniques, which are known as relatively low-cost trace analysis methods, are interesting alternatives to identify and quantify compounds such as morpholine in water from industrial activity providing high sensitivity, speed in analysis time, and portability [18,19].

A prerequisite for the successful implementation of electroanalytical techniques to the detection of a particular compound is to have an electrode that facilitates the electrochemical redox reactions of that given compound. Among the well-known and frequently used working electrodes, glassy carbon could be named, which for common solvents provides a large potential window in both anodic and cathodic regions. A good working electrode must possess electrochemical stability, electrical conductivity, voltammetric behaviour with a high signal-to-noise ratio, non-toxic nature and economic viability [20]. Combined with the intrinsic benefits of electroanalytical techniques, it is still possible to obtain improvements in relation to sensitivity, selectivity and linear relationship through modification of the electrode surface by materials such as carbon nanotube (CNT), graphene, metal particles, metal oxides and molecularly imprinted polymers [21,22].

In that context, carbon nanomaterials, such as CNTs and graphene, offer exclusive advantages in various aspects, like high surface-to-volume ratio, high electrical conductivity, great chemical and mechanical stability, and are gaining prominence [23–25]. Greater sensitivity and lower detection limits accessible with these nanomaterials for sensor applications are frequently reported and emphasized merits are compared with conventional options.

This work focused on the assessment of electrochemical sensors, starting from the widely-used glassy carbon electrode (GCE) as the reference, followed by the improvements in sensitivity, selectivity and the detection limit caused by the implementation of carbon nanomaterials, such as CNTs and graphene, enabling the determination of morpholine in synthetic boiler water (composed of $CaCO_3$, Na_2SO_3, Na_3PO_4 and $FeCl_3$).

2. Experimental

2.1 *Reagents*

The reagents used were: ammonium sulphate ($(NH_4)_2SO_4$ ≥99.0%, Sigma-Aldrich), *N,N*-dimethylformamide (C_3H_7NO, 99.0%, Sigma-Aldrich), morpholine P. A. (C_4H_9NO, 99.0%, Vetec), potassium chloride (KCl, ≥99.0%, Sigma-Aldrich), potassium ferricyanide ($K_3[Fe(CN)_6]$, ≥99.0%, Sigma-Aldrich), ferric chloride ($FeCl_3$, ≥99.99%, Sigma-Aldrich), sodium sulphite (Na_2SO_3, ≥98.0%, Sigma-Aldrich), sodium phosphate (Na_3PO_4, ≥98.0%, Sigma-Aldrich), calcium carbonate ($CaCO_3$, ≥99.0%, Sigma-Aldrich) and graphite sheet with 0.25 mm thickness (Alfa Aesar). All solutions were prepared in purified water by the Milli-Q Millipore system (resistivity ≥18 MΩ cm^2).

2.2 *Graphene synthesis*

Graphene was synthesized by electrochemical exfoliation in two electrodes set-up: a platinum wire as the counter electrode and a graphite sheet 0.25 mm (99.8%, Alfa Aesar) as the working electrode, and 0.1 mol l^{-1} $(NH_4)_2SO_4$ solution as the electrolyte. A potential difference (ddp) of 10 V was applied between the two electrodes for approximately 30 min until the graphite exfoliation process was completed. After exfoliation, the product was vacuum-filtered and washed repeatedly with water to remove any residual salts, and then the resulting material was dispersed in dimethylformamide (DMF) for 30 min in an ultrasound bath. The electrochemically exfoliated graphene was named EG.

2.3 *CNTs synthesis*

Procedures for preparing CNTs by chemical vapour deposition and subsequent purification were based on the works of Mazzocchia *et al* and Hou *et al* [26,27]. A metallic catalyst based on iron supported on neutral γ-alumina was used with an iron concentration of 9.5% (w/w). The arrangement of the tube in the oven was vertical, to provide the conditions for installing the fluidized bed. The hot zone of 40 cm was divided into two parts by a distribution plate: a 10 cm preheat zone and a second 30 cm fluidization zone. The reactor was heated at a rate of 10°C min^{-1}, from room temperature to 650°C, under an atmosphere consisting of 200 sccm of hydrogen (H_2) and 200 sccm of nitrogen (N_2) to establish the conditions of the fluidized channel. At

650°C, an isothermal phase of 45 min was followed in the same atmospheric conditions. In this stage, the calcined iron catalyst supported on alumina was activated by hydrogen reduction. Subsequently, a flow of 50 sccm of ethylene (C_2H_4) was introduced to the mixture for 60 min. The proportion of gases N_2 : H_2 : C_2H_4 was 4 : 4 : 1. These conditions correspond to the growth of CNTs on the activated iron catalyst. After 60 min growth time, the reactor was cooled down to room temperature under N_2 flow.

A procedure based on acid treatment was used for CNT purification. In the treatment, 5 g of synthesized CNTs were suspended in a 250 ml mixture of sulphuric and nitric acids (4 mmol l^{-1} H_2SO_4 and 1 mol l^{-1} HNO_3) and refluxed at 110°C for 5 h. During this stage, the dissolution of the alumina support, iron catalyst and amorphous carbon phases occurred, resulting in the purification of CNTs. Then, the suspension was stirred for 1 h, sonicated for 30 min and filtered. The filtered products were repeatedly immersed in distilled water, stirred, sonicated and refiltered until pH 7 was obtained in the filtered solution. Subsequently, the filtered products were dried at 100°C overnight.

2.4 *Electrode preparation; loading of EG and CNTs on GCE for morpholine determination*

Suspensions of EG and CNTs in DMF (1 mg ml^{-1}) were prepared by sonicating the mixture for 30 min. The modification of GCE was performed by adding three aliquots of 3 µl of suspension on the electrode surface, using an automatic volumetric pipette. Then, the electrode was kept for 15 min to dry in an oven at 40°C.

2.5 *Preparation of the synthetic boiler water*

A synthetic sample of boiler water was prepared due to the unavailability of a real sample, for analysis. The sample was prepared by adding the following salts: $CaCO_3$, Na_2SO_3, Na_3PO_4, $FeCl_3$ [8] at a concentration of 70 ppm for each salt in 15 ml of water.

2.6 *Electrochemical tests*

2.6a *Equipment*: The study of the electrochemical properties of the synthesized nanomaterials was performed on an AUTOLAB Potentiostat model PGSTAT 204 (Metrohm Autolab Utrecht, The Netherlands), controlled by Nova 1.11 software.

2.6b *Electrochemical analysis*: Electrochemical experiments for determination of morpholine were performed in a three-electrode set-up with a customized 50 ml cell, GCE/modified GCE (4 mm diameter, corresponding to 0.1256 cm^2 geometrical area) working electrode, Ag/AgCl (3 mol l^{-1} KCl) reference electrode, and a platinum wire counter electrode.

The electrochemical behaviour was studied by cyclic voltammetry, varying the scan rate from 10 to 100 mV s^{-1} and the electroactivity of the electrodes was investigated by differential pulse voltammetry (DPV), using an amplitude of 50 mV, a potential step of 10 mV, and a scanning speed 20 mV s^{-1}.

2.6c *Electroactive area study*: This study was carried out to estimate the electrochemically active surface area of the working electrode, using the Randles–Ševčík equation (1). For this purpose, cyclic voltammetry measurements were performed in a solution of 6.6 × 10^{-4} mol l^{-1} of $K_3[Fe(CN)_6]$ in 0.1 mol l^{-1} KCl at different scan rates.

$$Ip = 2.69 \times 10^5 n^{3/2} A C D^{1/2} v^{1/2}, \quad (1)$$

where I_p is the peak current (A), A is the electroactive area (cm^2), D is the diffusion coefficient of the hexacyanoferrate (III) anion ($[Fe(CN)_6]^{-3}$) in solution (6.20 × 10^{-6} cm^2 s^{-1}), n is the number of electrons involved in the redox reaction, v is the potential scan speed (V s^{-1}) and C is the concentration of the electroactive species (mol cm^{-3}).

2.7 *Characterization techniques of carbon nanomaterials*

X-ray photoelectron spectroscopy (XPS) analyses were performed in an ultra-high vacuum chamber (pressure: 10^{-9} mbar; Omicron Nanotechnology) using an anodic double X-ray source, Al (Kα = 1486.7 eV) with an anode voltage of 15 kV and filament current of 20 mA. The survey scans were obtained with 160 eV pass energy and 1 eV step size. The high-resolution spectra in the carbon region (C1s) were obtained with 20 eV analyzer pass energy and 0.05 eV step size.

Raman spectroscopy analyses were performed with a Witec Alpha 300 spectrometer, with a 532 nm laser line in a backscatter configuration using a microscope with a 100x objective. The laser power was kept below 0.5 mW to avoid local heat and damage to the samples. All spectra were acquired using 10 s of integration time and an average of 10 accumulations. The final spectrum was obtained by averaging three measurements taken at random points to assess material homogeneity.

X-ray diffraction (XRD) analyses were performed with a D8-Focus Bruker diffractometer using Ni-filtered Cu-Kα radiation (λ = 1.5406 Å) with a 0.02° step and a 2θ scan interval of 5 to 40°.

The transmission electron microscopy (TEM), and high-resolution TEM (HRTEM) analyses were carried out on a Titan 80-300 using an acceleration voltage of 80 kV to prevent the sample from electron irradiation damaging effects.

2.8 *Partial validation*

According to Ribani *et al* [28], the justification for the validation of analytical methods is based on legal, technical

and commercial reasons that aim to standardize the analytical methods of analysis, to guarantee the reliability of the marketed product or service, and show technical competence. The validation establishes that, through systematic studies of laboratory tests, the method is suitable for the intended purpose, that is, quantify the analyte content as close as possible to the real value. The partial validation of the studied method was carried out based on resolution international and Brazilian guidelines [29,30]. The parameters validation methods adopted, and the number of samples prepared for evaluation are described below.

3. Results

3.1 *Characterization of graphene and CNTs*

The surface morphologies of the nanomaterials were examined using TEM (figure 1a, c and d) and HRTEM (figure 1b).

The CNTs, synthesized by chemical vapour deposition, show a homogeneous size distribution with diameters in the range of 10 to 15 nm (figure 1a). Figure 1b allows a more accurate analysis of the structure of the synthesized CNTs, with the presence of parallel cylindrical graphene layers around a central cavity, confirming the multi-walled structure of the CNTs. Figure 1c and d shows the GE images, where it is possible to observe micrometre-sized graphene sheets, presenting typical wrinkles on the thin 2D foils of the material.

Figure 2 shows the results of the Raman analyses performed on the EG and CNT samples.

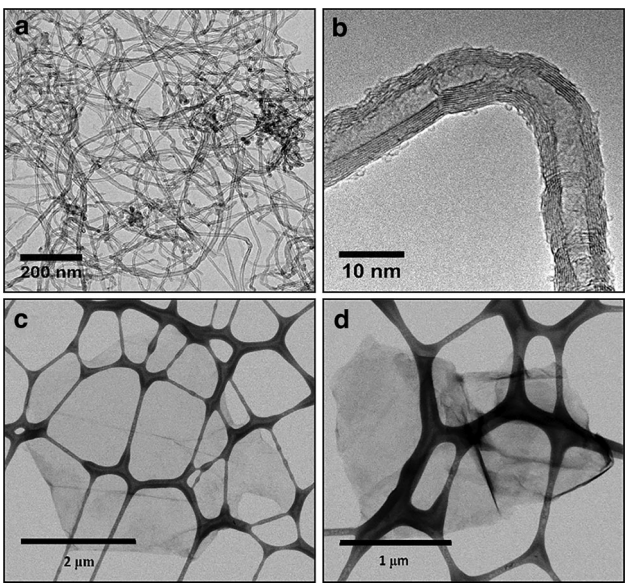

Figure 1. (**a**, **b**) TEM and HRTEM images, respectively, of CNTs and (**c**, **d**) TEM images of EG, on the copper grid covered by a lacy carbon film.

Raman spectra of the studied samples exhibit the bands typical for carbon-based materials (figure 2). The band at approximately 1350 cm $^{-1}$, also called the D-band, reflects the presence of disorder or defects in the lattice, such as vacancies, functional groups like oxygen-containing groups, or even adsorption of molecules on their surface. The second band, called the G-band, originates from the vibration mode of stretching carbon atoms in the plane with sp^2 hybridization, common in graphitic structures [31–33]. The bands positioned near 2700 and 2900 cm^{-1} are known as a contribution of the second-order of D-band and a combination of G and D bands, respectively.

The position of the G-band (or 2D) is not the same for EG and CNT, it is due to the difference in the type and level of interactions between the layers of graphene stacked on both materials and the different number of layers (the way it affects the D). Both structures have some degree of defects, but the type and density of defects are different. The Raman spectra shows that the number of layers is higher in EG [32,34–36].

The ID/IG ratio has been used to assess the degree of defects in a graphite structure. In general, the intensity of the D-band is considered dependent on the defects that exist in the structure. The greater the intensity of the D-band, the greater the number of defects in the structure [37]. As observed in the spectra presented, both CNT and GE have very pronounced D-bands, indicating a considerable amount of defects that, in the case of CNT, come from the functionalization step. According to figure 2, the ID/IG ratio was higher for CNTs.

XPS analyses were performed to study the chemical environment of the samples' surface, the oxidation level and quality of the samples. The survey spectra of CNT and EG (figure 3) show only carbon and oxygen constituents present. Quantification of the data reveals a lower oxygen content in the CNT sample (C content of 96.4 at%) compared with EG (C content of 85.9 at%). No unexpected

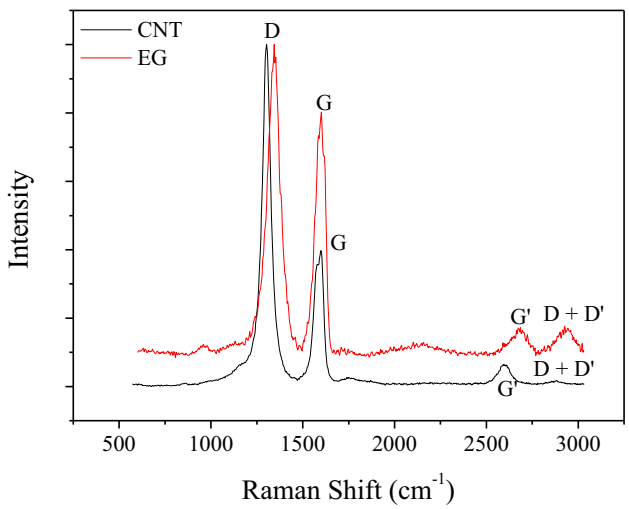

Figure 2. Raman spectra of EG and CNT samples.

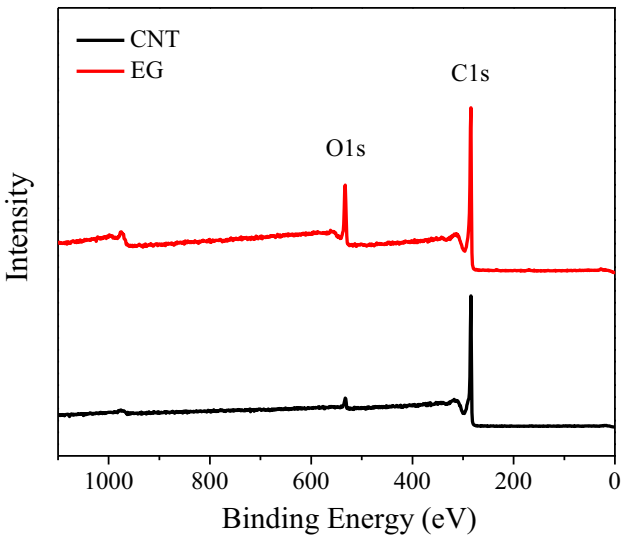

Figure 3. Survey spectra of the CNT and EG samples.

impurities were detected and therefore, within the detection limit of the technique (∼1 at%), the preparation and purification procedures are considered capable of delivering acceptable quality samples.

High-resolution C1s spectra of EG and CNT samples are shown in figure 4, where the degree of oxidation and the type of functional groups could be evaluated. Deconvolution of the C1s spectra was conducted according to the following positions for the corresponding transitions; C=C aromatic (sp^2 carbon, 284.6 eV), C–C (sp^3 carbon, 285.1 eV); C–OH (alcohol, 285.6 eV); C–O–C (ether, 286.8 eV); C=O (carbonyl, 288.6 eV); COOH (carboxyl, 289.8 eV) and satellite peak (shake-up, 291.5 eV) [33,38,39]. The deconvolution results showed a greater amount of oxygen functional groups in GE sample compared to the CNT sample, but still, the contribution of C=C bonds is practically dominant in the EG sample. Thus, it is observed that the material produced by electrochemical exfoliation is partially oxidized. Notwithstanding the negative effect of such groups on the electrical properties of carbonaceous materials, a controlled level of their concentration could have positive effects on the electrochemical performance. For instance, due to improved wettability, higher level of electrode–electrolyte interactions, and more homogenous electroactive layer formation when the GCE is used as the current collector for conducting the electrochemical analysis. Electrodes with homogenous films have greater stability and reproducibility in the results [33,40].

The EG and CNT XRD patterns showed a peak at $2\theta \approx 26.33–26.5^{\circ}$ (figure 5), corresponding to the (002) planes of hexagonal graphite. The higher relative intensity of the CNT signals indicated a higher crystallinity compared to graphene. The broader (002) peak for EG can be related to the small crystallite size, and a large number of structural defects and/or functional groups, which promote the loss of structure periodicity [33].

3.2 *Study of the electroactive area of the electrodes modified with the EG and CNT films*

The voltammograms and analytical curves obtained for the electroactive area study could be seen in the supplementary material (see supplementary figures S1, S2 and S3). There is a linear relationship between anodic peak current values ($I_{p,a}$) with the square root of the scan rate. The angular coefficients of the linear regression (in I_p *vs.* $v^{1/2}$ plot) obtained for GCE, GCE–EG and GCE–CNT were 1.67×10^{-4}, 2.85×10^{-4} and 2.51×10^{-4}, respectively. Using equation (1) and the angular coefficients obtained, it was possible to estimate the active area of the studied electrodes. The values of electroactive area for the studied electrodes are shown in table 1.

Table 1 suggests an increase of the GCE active area by factors of 1.7 and 1.5 with EG and CNT, respectively. This

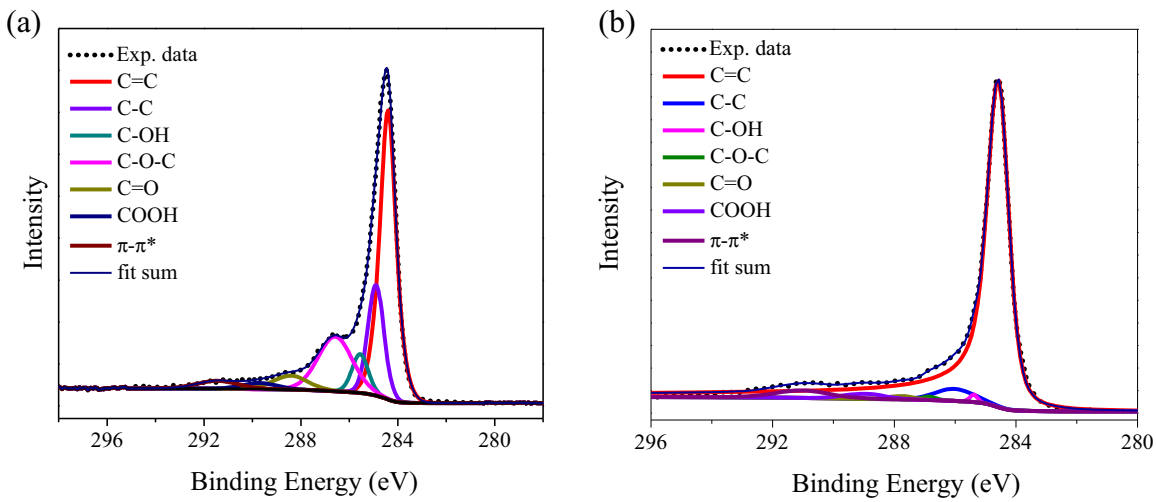

Figure 4. High-resolution C1s spectra of (**a**) EG and (**b**) CNT samples.

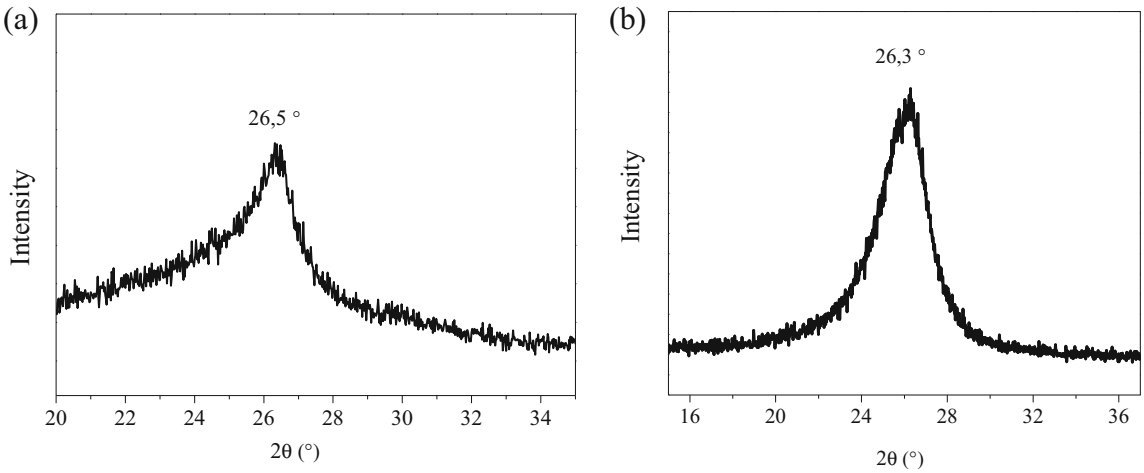

Figure 5. X-ray diffraction patterns of (**a**) EG and (**b**) CNT samples.

Table 1. Calculated values of electroactive area for the GCE, GCE–EG and GCE–CNT electrodes.

Redox indicator	GCE (cm^2)	GCE–EG (cm^2)	GCE–CNT (cm^2)
Potassium hexacyanoferrate (III)	0.38	0.65	0.56

Geometric area: 0.1256 cm^2.

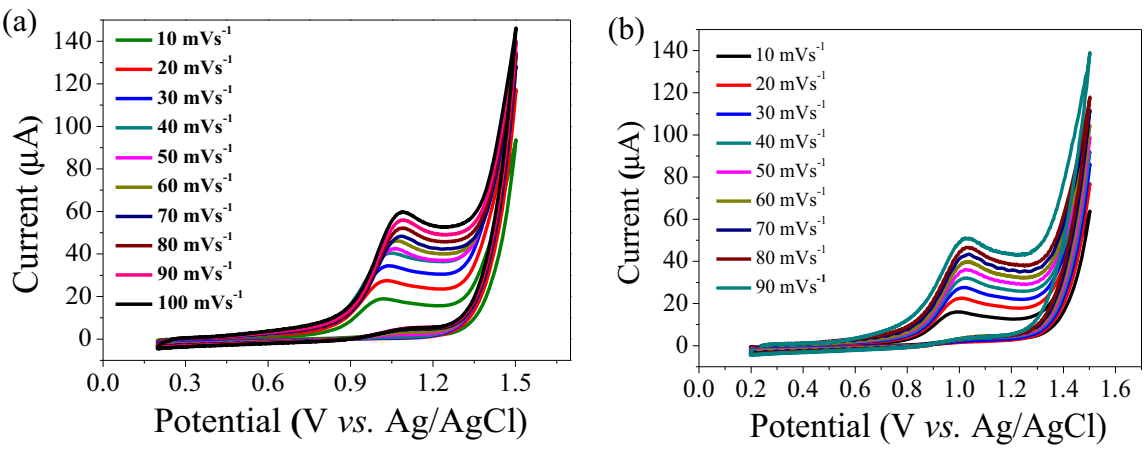

Figure 6. Cyclic voltammograms for 80 mg l^{-1} of morpholine, in an electrolyte solution in 0.1 mol l^{-1} of KCl (pH 10) varying the scan speed from 10 to 90 mV s^{-1} using (**a**) GCE–EG and (**b**) GCE–CNT.

increase can be attributed to the increase in the global surface area of the electrode and in turn, the increased electroactive sites provided by EG and CNT.

3.3 *Study of the electroactivity of the electrodes modified with the EG and CNT films*

For a better understanding of the mechanism involved in the electrochemical process of morpholine, the cyclic voltammetry technique was performed in a 0.1 mol l^{-1} KCl solution (pH 10) in the presence of 80 mg l^{-1} of morpholine, varying the speed of 10 to 100 mV s^{-1} scan, as shown in figure 6.

For both, there is a single anodic peak, and the morpholine oxidation potential shifts to more positive values with increase in scan speed, indicating characteristics of an irreversible process [41]. This behaviour is already in agreement with the electrooxidation mechanism proposed in the literature by the electrooxidation of morpholine using

a boron-doped diamond electrode [8]. The irreversible process can be explained because the produced radical is likely very unstable with a low life and therefore does not support reverse electron transfer (Reaction I [8]).

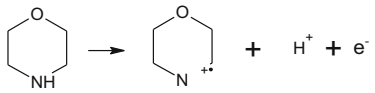

(Reaction I)

Through the construction of the curve studying the variation of the anodic peak *vs*. the square root of the scan rate, a linear profile was obtained for both curves indicating that the process is controlled by diffusion.

The electroactivity of the electrodes towards morpholine detection was investigated over a potential range of 0.5 to 1.45 V *vs.* Ag/AgCl. Figure 7 shows the voltammograms obtained with different electrodes in the presence of 80 mg l^{-1} of morpholine in 0.1 mol l^{-1} KCl, pH 10 at a scan rate of 20 mV s^{-1}.

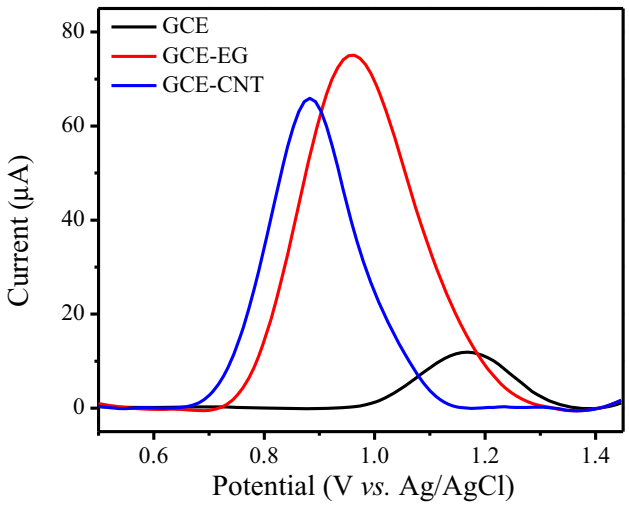

Figure 7. Voltammograms obtained by differential pulse voltammetry in the presence of 80 mg l^{-1} of morpholine, using GCE, GCE–EG and GCE–CNT, in 0.1 mol l^{-1} of KCl (pH 10).

The presence of an anodic peak was observed at approximately +1.2 $V_{Ag/AgCl}$ using GCE. EG and CNT electrodes improved the performance by decreasing the oxidation potential (+0.85 and +0.95 $V_{Ag/AgCl}$, for CNT and EG, respectively) and increasing the peak current. This indicates that the CNT electrode is more electroactive for the oxidation of morpholine.

Figure 8 shows the relationship between the electrochemical charge associated with anodic peaks (in µC) and the morpholine concentration (in mg l^{-1}) over the concentration range of 12–82 mg l^{-1}, in KCl 0.1 mol l^{-1}, pH 10, using GCE–EG and GCE–CNT. A good linear relationship with a reasonable correlation coefficient is seen for both EG and CNT electrodes (r = 0.9804 and 0.9871, respectively).

Through figure 8, it is possible to notice that the GCE–EG electrode is more sensitive than the GCE–CNT electrode. This result was already expected because although the GCE-EG electrode presents a lower potential displacement, it presented a higher electroactive area, and the area influences the electrode sensitivity.

3.4 *Detection and quantification limits*

Table 2 presents the limits of detection (LOD) and limits of quantification (LOQ) determined using equation LD = 3.3 ($\sigma c/\alpha$), where LD is the detection limit, σc is the standard deviation of the analytical curve intercept and α is the slope of the analytical curve. The quantification limit was estimated as three times the detection limit. The obtained analytical parameters are summarized in table 2. The LOD and LOQ results obtained were superior to other electrochemical methods available in the literature; however, they were inferior to the chromatographic and

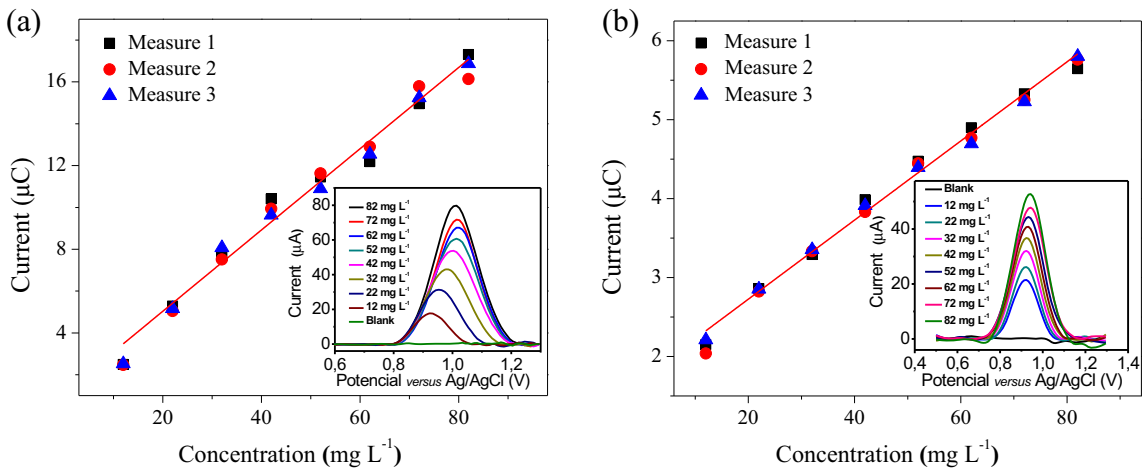

Figure 8. Analytical curves were obtained for evaluating the linear range of the morpholine oxidation response in 0.1 mol l^{-1} KCl, pH 10 at 20 mV s^{-1}, using (**a**) GCE–EG and (**b**) GCE–CNT electrodes.

Table 2. Limits of detection and quantification obtained for GCE–EG and GCE–CNT.

Electrode	LOD (mg l^{-1})	LOQ (mg l^{-1})
GCE–EG	1.1	3.3
GCE–CNT	1.3	3.9

spectrophotometric methods (table 3). Although the proposed method has higher LOD and LOQ values than the classic methods, the presented method has the advantage of being faster, cheaper, there is no need for pre-treatment of the sample, and is less laborious, indicating that it is an excellent alternative for detection and quantification of morpholine.

3.5 *Precision*

In this study, the precision of the developed method was evaluated based on the relative standard deviation of repeatability and from the intermediate precision.

3.5a *Repeatability*: The relative standard deviation, for the GCE–EG, is shown in table 4 for the analytical curve presented in figure 8a, and presented a recovery variation from 84 to 111%.

The GCE–CNT relative standard deviation is shown in table 5 for the analytical curve presented in figure 8b. The electrode presented a recovery variation from 98 to 104%.

The repeatability tests obtained for GCE–EG and GCE–CNT showed that according to literature these sensors are acceptable to analytical methods [30,42,45].

3.5b *Intermediary precision*: For intermediary precision, the variances obtained from the experiments with the same analytes and the same GCE–EG and GCE–CNT electrodes (figure 9a and b) and under the same analysis conditions, on different days, were used to calculate the F-values. The results, i.e., 0.002 and 0.02 for EG and CNT, respectively, were lower than the critical F-value (4.60) for a 95% confidence level, indicating equal variances. The slopes of the analytical curves were also compared; the calculated *t*-values (0.90 and 1.50 for EG and CNT, respectively) were lower than the critical *t*-value (2.36) for a 95% confidence level, indicating equal slopes for these two curves.

The intermediate precision was also obtained from the same analyst using different modified GCE–GE and GCE–CNT electrodes (figure 10a and b) under the same analysis conditions, on different days. The calculated F-values (0.03 for both electrodes) were lower than the critical F-value (4.60) for a 95% confidence level, indicating equal variances. The slopes of the analytical curves were also compared; the calculated *t*-value (0.19 and 1.56 for EG and

Table 3. Comparative of previously reported methods for detecting morpholine.

Methods		LOD (mg l^{-1})	LOQ (mg l^{-1})	References
Screen-printed carbon electrode	—	10	33	[42]
Screen-printed carbon electrode	Indirect determination	1.0	3.3	[9]
Platinum microelectrode	—	12	40	[43]
Spectrophotometry	Derivatization	1.0	3.3	[44]
Boron-doped diamond electrode	—	2.1	6.9	[8]
Liquid chromatography	Derivatization	0.01	0.033	[12]
Gas chromatography-mass spectrometry	Derivatization	0.0073	0.024	[17]

Table 4. Recovery results using GCE–EG.

Theoretical [morpholine] (mg l^{-1})	1st signal (μC)	2nd signal (μC)	3rd signal (μC)	Average (μC)	Measured [morpholine] (μC)	Relative standard deviation (%)	Recovery (%)
12	2.48	2.46	2.52	2.45	2.91	1.36	84
22	5.28	5.05	5.16	5.16	4.96	2.24	104
32	7.68	7.51	8.07	7.75	7.01	3.74	111
42	10.4	9.93	9.62	9.99	9.06	3.91	110
52	11.5	11.6	10.9	11.3	11.1	3.37	102
62	12.2	12.9	12.5	12.5	13.2	2.87	95
72	15.0	15.8	15.2	15.3	15.2	2.75	101
82	17.3	16.1	16.9	16.8	17.3	3.52	97

Table 5. Recovery results using the GCE–CNT.

Theoretical [morpholine] (mg l^{-1})	1st signal (μC)	2nd signal (μC)	3rd signal (μC)	Average (μC)	Measured [morpholine] (μC)	Relative standard deviation (%)	Recovery (%)
12	2.15	2.04	2.21	2.13	2.18	4.12	98
22	2.86	2,82	2,85	2.85	2.71	0.70	105
32	3.29	3.33	3.35	3.32	3.24	0.94	103
42	3.99	3.83	3.91	3.91	3.76	2.01	104
52	4.47	4.45	4.39	4.44	4.29	0.93	103
62	4.90	4.77	4.69	4.79	4.82	2.15	99
72	5.33	5.25	5.23	5.27	5.34	1.00	99
82	5.65	5.76	5.80	5.74	5.87	1.40	98

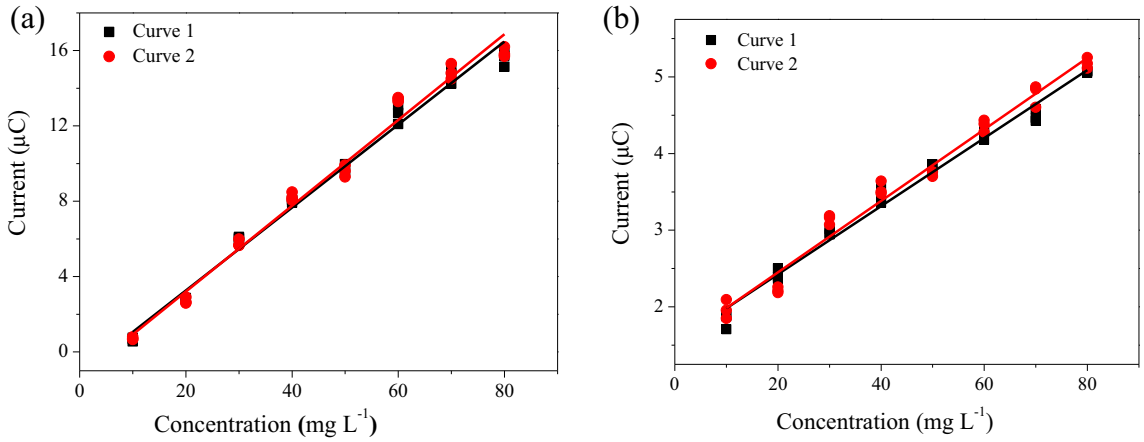

Figure 9. Precision study for the proposed voltammetric method using the analytical curves obtained with the same analyst using the same electrodes: (**a**) GCE–EG and (**b**) GCE–CNT.

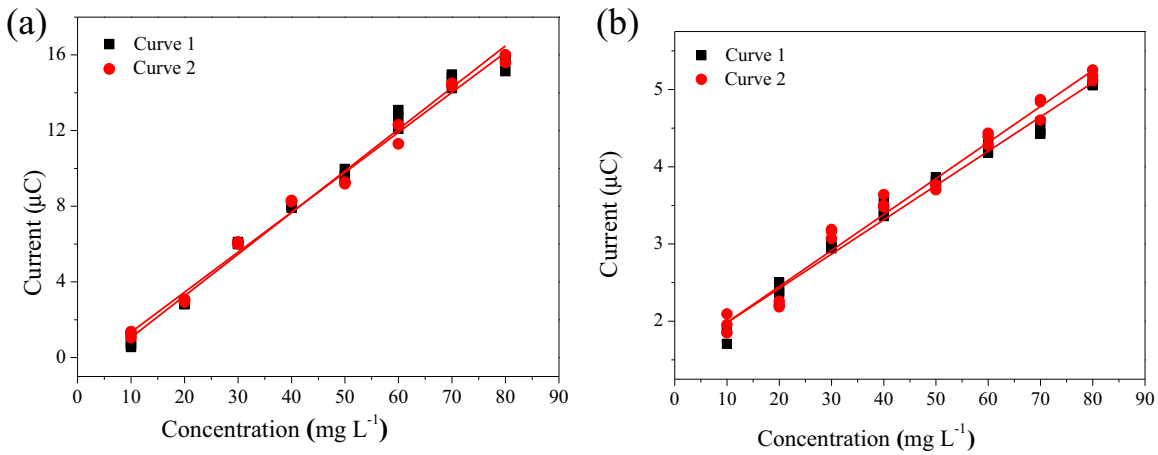

Figure 10. Precision study for the voltammetric method using analytical curves obtained with same analyst using different modified (**a**) GCE–EG and (**b**) GCE–CNT electrodes.

CNT, respectively) were lower than the critical *t*-value (2.36) for a 95% confidence level, indicating equal slopes for these two curves.

The intermediary precision studies show that all the prepared films present high reproducibility.

3.6 *Sample recovery*

In figure 11, it is possible to observe the voltammogram of the quantification of morpholine using GCE–EG and GCE–CNT.

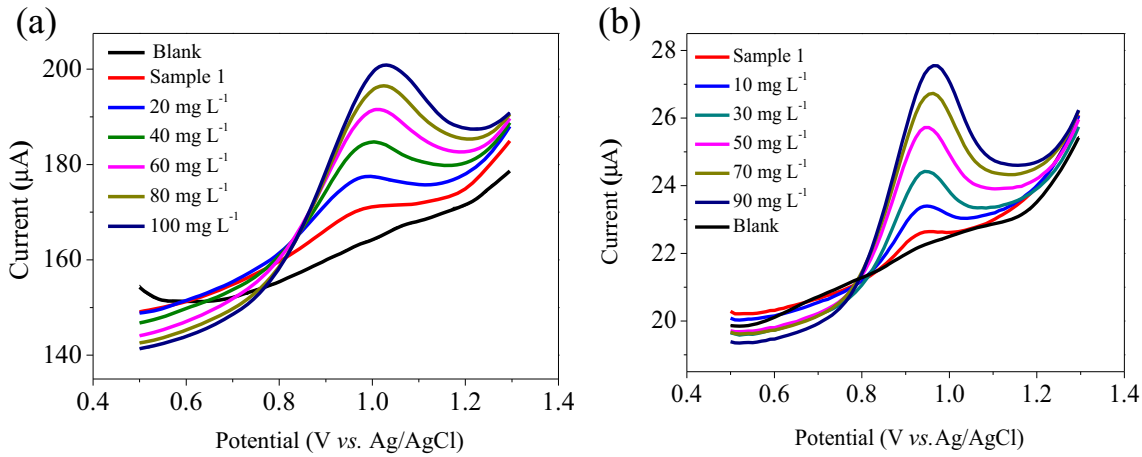

Figure 11. Differential pulse voltammogram obtained in the standard addition analysis using the sample with (**a**) GCE–EG and (**b**) GCE–CNT in 0.1 mol l^{-1} KCl, at pH 10, at 20 mV s^{-1}.

Table 6. Determination of morpholine in synthetic boiler water using GCE–EG and GCE–CNT. The results are expressed as mean ± standard deviation (n = 3).

Sample	Theoretical concentration (mg l^{-1})	Analysed concentration (mg l^{-1})	Recovery (%)
GCE–EG Sample 1	10.0	11.63 ± 2.82	116.3
GCE–EG Sample 2	20.0	21.39 ± 2.49	107.0
GCE–CNT Sample 1	10.0	11.45 ± 1.34	114.5
GCE–CNT Sample 2	20.0	20.62 ± 3.31	103.1

For the study of the recovery of the synthetic sample, boiler water without morpholine was added to the blank. As can be seen in figure 11, for both electrodes in the blank, no peak was observed, showing that the system matrix (composed of $CaCO_3$, Na_2SO_3, Na_3PO_4 and $FeCl_3$) does not influence the morpholine analysis, indicating the method selectivity. The results obtained in this study of recovery are shown in table 6.

Both GCE–EG and GCE–CNT sensors showed a good recovery of 107 and 103% at 20.0 mg l^{-1}.

4. Conclusion

Two carbonaceous nanomaterials were proposed in this study as efficient candidates for quantification of morpholine in electrochemical sensors, namely, electrochemically exfoliated graphene and chemical vapour deposition synthesized multi-walled carbon nanotubes. Synthesis and microstructural characterization of the above materials were carried out and subsequent electrochemical performance of the electrodes made of them was demonstrated.

The electrochemical studies proved the efficient behaviour of the electrodes made of EG and CNT (GCE-EG and GCE-CNT, respectively) in sensing and detection of morpholine via differential pulse voltammetry. The area of the anodic peaks was well correlated with the concentration of the analyte, which enabled the construction of analytical curves with good linear correlation coefficients for the studied concentration range. It was observed that implementation of a thin film of EG and CNT on the GCE, promoted the electrocatalytic activity towards morpholine electro-oxidation, and a considerable increase in the corresponding oxidation peak was observed in both cases.

Theoretical detection limits of 1.0 and 1.3 mg l^{-1} were obtained for GCE–EG and GCE–CNT, respectively. These merit figures, both satisfactorily meet the requirements of the Food and Drug Administration for morpholine detection in real applications.

The recovery figures observed for GCE–EG and GCE–CNT sensors were in the range 84–111% and 98–104%, respectively, fitting well within the acceptable range of 70 to 120%. Besides, the sample recovery for GCE–EG and GCE–CNT sensors were 107 and 103%, respectively, at 20.0 mg l^{-1} morpholine.

Acknowledgements

We thank Fundação de Amparo à Pesquisa do Estado do Rio de Janeiro (FAPERJ), Coordenação de Aperfeiçoamento de Pessoal de Nível Superior (CAPES) and Conselho Nacional de Desenvolvimento Científico e Tecnológico (CNPq) for financial support.

References

[1] Kuchowicz E and Rydzyński K 2011 *Appl. Occup. Environ. Hyg.* **13** 113
[2] Moger M, Satam V, Govindaraju D R C, Paniraj A S, Gopinath V S, Hindupur R M *et al* 2014 *J. Braz. Chem. Soc.* **25** 104
[3] Kourounakis A P, Xanthopoulos D and Tzara A 2020 *Med. Res. Rev.* **40** 709
[4] Ghafari S, Ranjbar S, Larijani B, Amini M, Biglar M, Mahdavi M *et al* 2019 *Int. J. Biol. Macromol.* **135** 978
[5] Zhao C, Zhou J, Gu Y, Pan E, Sun Z, Zhang H *et al* 2020 *Sci. Total Environ.* **738** 139713
[6] Rath S and Canaes L S 2009 *Quim. Nova* **32** 2159
[7] Shea T E J 1939 *J. Ind. Hyg. Toxicol.* **21** 236
[8] Rocha L R, D'Elia E, Medeiros R A and Tarley C R T 2018 *Anal. Lett.* **52** 1083
[9] Kolliopoulos A V, Metters J P and Banks C E 2015 *Environ. Sci. Water Res. Technol.* **1** 40
[10] Gilbert R, Rioux R and Saheb S E 2002 *Anal. Chem.* **56** 106
[11] Lamarre C, Gilbert R and Gendron A 1989 *J. Chromatogr. A* **467** 249
[12] Joseph M, Kagdiyal V, Tuli D K, Rai M M, Jain S K, Srivastava S P *et al* 1993 *Chromatographia* **35** 173
[13] Vatsala S, Bansal V, Tuli D K, Rai M M, Jain S K, Srivastava S P *et al* 1994 *Chromatographia* **38** 456
[14] Pietsch J, Hampel S, Schmidt W, Brauch H-J and Worch E 1996 Fresenius. *J. Anal. Chem.* **355** 164
[15] Luong J, Shellie R A, Cortes H, Gras R and Hayward T 2012 *J. Chromatogr. A* **1229** 223
[16] Chen D, Miao H, Zou J, Cao P, Ma N, Zhao Y *et al* 2015 *J. Agric. Food Chem.* **63** 485
[17] Cao M, Zhang P, Feng Y, Zhang H, Zhu H, Lian K *et al* 2018 *J. Anal. Methods Chem.* **2018** 1
[18] Beitollahi H, Dourandish Z, Tajik S, Ganjali M R, Norouzi P and Faridbod F 2018 *J. Rare Earths* **36** 750
[19] Paiva V M, Assis K L S C, Archanjo B S, Senna C A, Ribeiro E S and D'Elia E 2021 *Bull. Mater. Sci.* **44** 14
[20] Pletcher D, Greff R, Peat R, Peter L M and Robinson J 2010 in *Instrumental methods in electrochemistry* (Cambridge: Woodhead Publishing) p 15
[21] Edwards G A, Bergren A J and Porter M D 2007 in *Handbook of electrochemistry* (ed C Zoski) (Amsterdam: Elsevier) p 295
[22] Ratajczak P, Suss M E, Kaasik F and Béguin F 2019 *Energy Storage Mater.* **16** 126
[23] Tajik S, Dourandish Z, Zhang K, Beitollahi H, Le Q V, Jang H W *et al* 2020 *RSC Adv.* **10** 15406
[24] Thi Mai Hoa L 2018 *Diam. Relat. Mater.* **89** 43
[25] Patra S, Roy E, Madhuri R and Sharma P K 2016 *Anal. Chim. Acta* **918** 77
[26] Mazzocchia C V, Bestetti M, Acierno D and Tito A 2010 *Eur. Patent* 2213369A1
[27] Hou P X, Liu C and Cheng H M 2008 *Carbon N. Y.* **46** 2003
[28] Ribani M, Bottoli C B G, Collins C H, Jardim I C S F and Melo L F C 2004 *Quim. Nova* **27** 771
[29] U.S. Departament of Health and Human Services 1996 *Q2B Validation of analytical procedures: methodology*. http://www.fda.gov/cder/guidance/index.htm or http://www.fda.gov/cber/guidelines.htm
[30] Rego E C P 2016 *Orientação sobre validação de métodos analíticos - DOQ-CGCRE-008. Instituto Nacional de Metrologia, Qualidade e Tecnologia (INMETRO)* 1
[31] Dennison J, Holtz M and Swain G 1996 *Spectroscopy* **11** 38
[32] Ferrari A C 2007 *Solid State Commun.* **143** 47
[33] Castro K L S, Curti R V, Araujo J R, Landi S M, Ferreira E H M, Neves R S *et al* 2016 *Thin Solid Films* **610** 10
[34] Malard L M, Pimenta M A, Dresselhaus G and Dresselhaus M S 2009 *Phys. Rep.* **473** 51
[35] Ferrari A C and Basko D M 2013 *Nat. Nanotechnol.* **8** 235
[36] Dresselhaus M S, Jorio A, Hofmann M, Dresselhaus G and Saito R 2010 *Nano Lett.* **10** 751
[37] Antunes E F, Lobo A O, Corat E J, Trava-Airoldi V J, Martin A A and Veríssimo C 2006 *Carbon N. Y.* **44** 2202
[38] Lesiak B, Kövér L, Tóth J, Zemek J, Jiricek P, Kromka A *et al* 2018 *Appl. Surf. Sci.* **452** 223
[39] Al-Gaashani R, Najjar A, Zakaria Y, Mansour S and Atieh M A 2019 *Ceram. Int.* **45** 14439
[40] dos Assis K L S C, Archanjo B S, Achete C A and D'Elia E 2020 *Mater. Res.* **23** 20190513
[41] Erden P E, Taşdemir I H, Kaçar C and Kiliç E 2014 *Int. J. Electrochem. Sci.* **9** 2208
[42] de Oliveira S M, Siguemura A, Lima H O, Souza F C, Magalhães A A O, Toledo R M *et al* 2014 *J. Braz. Chem. Soc.* **25** 1399
[43] de Oliveira S M, de Carvalho F S, Lima H O, Maciel R, Toledo R M, Augusto A *et al* 2015 *Int. J. Electrochem. Sci* **10** 5013
[44] Stevens W H and Skov K 1965 *Analyst* **90** 182
[45] Tehrani R M A and Ab Ghani S 2012 *Electrochim. Acta* **70** 153